Contribution from the Department of Chemistry, Harvard University, Cambridge, Massachusetts 02138, and the Francis Bitter National Magnet Laboratory, Massachusetts Institute of Technology, Cambridge, Massachusetts 02139

Analogues of the [4Fe-4S]$^+$ Sites of Reduced Ferredoxins: Structural and Spectroscopic Properties of $[(C_2H_5)_4N]_3[Fe_4S_4(S\text{-}p\text{-}C_6H_4Br)_4]$ in Crystalline and Solution Phases

D. W. STEPHAN,[1a,b] G. C. PAPAEFTHYMIOU,[1c] R. B. FRANKEL,[1c] and R. H. HOLM*[1b]

Received August 17, 1982

The structural properties of the reduced clusters $[Fe_4S_4(SR)_4]^{3-}$, synthetic analogues of the [4Fe-4S]$^+$ sites in ferredoxin proteins, have been augmented by preparation and single-crystal X-ray analysis of the title compound. $(Et_4N)_3[Fe_4S_4(S\text{-}p\text{-}C_6H_4Br)_4]$ (**1**) crystallizes in orthorhombic space group *Fdd*2 with $a = 36.218$ (10) Å, $b = 30.972$ (7) Å, $c = 11.631$ (3) Å, and $Z = 8$. The cluster has an imposed twofold symmetry axis and exhibits a distortion from idealized T_d symmetry of the [4Fe-4S]$^+$ core that is different from those of $(Et_3MeN)_3[Fe_4S_4(SPh)_4]$ (**2**) and $(Et_4N)_3[Fe_4S_4(SCH_2Ph)_4]$ (**3**), the only other structurally defined reduced clusters. One description of the cubane-type core involves four short and eight long Fe-S bonds with mean values of 2.292 (2) and 2.313 (8) Å, respectively. Solid **1** exhibits an especially well-resolved Mössbauer spectrum at 4.2 K consisting of two doublets of ~1:1 intensity having isomer shifts consistent with the mean oxidation state $Fe^{2.25+}$ and a quadrupole splitting difference of 1.13 mm/s. This spectrum is distinguishable from those of **2** and **3**. Internal hyperfine fields at the two resolvable Fe sites have been estimated from an analysis of magnetically perturbed spectra. The solution spectrum of **1** at 4.2-77 K is the same as those of all other $[Fe_4S_4(SR)_4]^{3-}$ clusters examined previously. These closely resemble that of **2**, which has a tetragonally elongated core structure, indicating a change to, or nearly to, this configuration upon passing from the solid to the solution state. This conclusion is also reached by comparison of EPR spectra in the two states. Compound **1** is the third containing a structurally characterized reduced cluster and sixth overall to exhibit, by magnetic and/or spectroscopic property/structure correlations, this structural change. The results of this investigation further substantiate the unperturbed structural change

$$[Fe_4S_4(SR)_4]^{2-}\ (\text{compressed } D_{2d}) \underset{-e^-}{\overset{+e^-}{\rightleftharpoons}} [Fe_4S_4(SR)_4]^{3-}\ (\text{elongated } D_{2d})$$

attendant to electron transfer. This redox couple is isoelectronic with the prevalent electron-transfer process of ferredoxins containing [4Fe-4S] sites.

Introduction

The prevalent electron-transfer process of ferredoxin (Fd) proteins containing cubane-type [4Fe-4S] redox sites[2] is that represented by the couple (1). The corresponding isoelectronic

$$Fd_{ox}([4Fe\text{-}4S]^{2+}) + e^- \rightleftharpoons Fd_{red}([4Fe\text{-}4S]^{+}) \quad (1)$$

$$[Fe_4S_4(SR)_4]^{2-} + e^- \rightleftharpoons [Fe_4S_4(SR)_4]^{3-} \quad (2)$$

couple of synthetic analogues of these sites is (2). Isolation of examples of both oxidized[3,4] and reduced[4-8] members of the latter couple has permitted investigation of several important features of cluster electron transfer. Chief among these are the fast electron self-exchange rates ($k \sim 10^6$-10^7 M^{-1} s^{-1} at ~298 K[9]) and the structural change attendant to electron transfer.[7,8] The latter is depicted schematically in Figure 1, where it is seen that the principal alteration is compression/elongation of the [4Fe-4S] core along the idealized $\bar{4}$ axis.

Evidence for the structural change in Figure 1 has been derived[7,8] from the following observations. (i) Crystal structures of some seven compounds containing clusters with the [4Fe-4S]$^{2+}$ core oxidation level[4,10-16] reveal the dominant deviation from idealized core T_d symmetry to have the form of a compressed tetragonal distortion. This distortion, while variable in extent, persists in quite different crystalline environments[12] and in clusters whose terminal ligands are wholly[10-13] or partially[14] thiolates or are other groups entirely.[15,16] Hence, the compressed D_{2d} structure appears to be the intrinsically stable form of the [4Fe-4S]$^{2+}$ core.[17] (ii) Distortions of the [4Fe-4S]$^+$ cores in crystalline $(Et_3MeN)_3[Fe_4S_4(SPh)_4]$[7] and $(Et_4N)_3[Fe_4S_4(SCH_2Ph)_4]$[18] are different from each other (Figure 1), and their solid-state magnetic and spectroscopic properties are distinct.[7] With use of these structure/property correlations, nine compounds of seven clusters $[Fe_4S_4(SR)_4]^{3-}$ have been broadly classified as containing elongated tetragonal or nontetragonal core structures in the solid state.[8] (iii) Regardless of their classification, spectroscopic and magnetic properties of all clusters in frozen solutions are essentially the same and are in agreement with those of crystalline $(Et_3MeN)_3[Fe_4S_4(SPh)_4]$, in which the

(1) (a) National Science and Engineering Research Council of Canada/NATO Postdoctoral Fellow, 1980-1982. (b) Harvard University. (c) MIT.
(2) Sweeney, W. V.; Rabinowitz, J. C. *Annu. Rev. Biochem.* **1980**, *49*, 139.
(3) Holm, R. H. *Acc. Chem. Res.* **1977**, *10*, 427. Holm, R. H.; Ibers, J. A. In "Iron-Sulfur Proteins"; Lovenberg, W., Ed.; Academic Press: New York, 1977; Vol. III, Chapter 7.
(4) Berg, J. M.; Holm, R. H. In "Metal Ions in Biology"; Spiro, T. G., Ed.; Wiley: New York, 1972; Vol. 4, Chapter 1.
(5) Cambray, J.; Lane, R. W.; Wedd, A. G.; Johnson, R. W.; Holm, R. H. *Inorg. Chem.* **1977**, *16*, 2565.
(6) Reynolds, J. G.; Laskowski, E. J.; Holm, R. H. *J. Am. Chem. Soc.* **1978**, *100*, 5315.
(7) Laskowski, E. J.; Frankel, R. B.; Gillum, W. O.; Papaefthymiou, G. C.; Renaud, J.; Ibers, J. A.; Holm, R. H. *J. Am. Chem. Soc.* **1978**, *100*, 5322.
(8) Laskowski, E. J.; Reynolds, J. G.; Frankel, R. B.; Foner, S.; Papaefthymiou, G. C.; Holm, R. H. *J. Am. Chem. Soc.* **1979**, *101*, 6562.
(9) Reynolds, J. G.; Coyle, C. L.; Holm, R H. *J. Am. Chem. Soc.* **1980**, *102*, 4350.
(10) $(Et_4N)_2[Fe_4S_4(SCH_2Ph)_4]$: Averill, B. A.; Herskovitz, T.; Holm, R. H.; Ibers, J. A. *J. Am. Chem. Soc.* **1973**, *95*, 3523.
(11) $(Me_4N)_2[Fe_4S_4(SPh)_4]$: Que, L., Jr.; Bobrik, M. A.; Ibers, J. A.; Holm, R. H. *J. Am. Chem. Soc.* **1974**, *96*, 4168.
(12) $Na_4(n\text{-}Bu_4N)[Fe_4S_4(SCH_2CH_2CO_2)_4]\cdot 5C_5H_9NO$: Carrell, H. L.; Glusker, J. P.; Job, R.; Bruice, T. C. *J. Am. Chem. Soc.* **1977**, *99*, 3683.
(13) $(Me_4N)_2[Fe_4S_4(SCH_2CH_2OH)_4]$: Christou, G.; Garner, C. D.; Drew, M. G. B.; Cammack, R. *J. Chem. Soc., Dalton Trans.* **1981**, 1550.
(14) $(Ph_4P)_2[Fe_4S_4(SPh)_2Cl_2]$: Coucouvanis, D.; Kanatzidis, M.; Simhon, E.; Baenziger, N. C. *J. Am. Chem. Soc.* **1982**, *104*, 1874.
(15) $(Et_4N)_2[Fe_4S_4Cl_4]$: Bobrik, M. A.; Hodgson, K. O.; Holm, R. H. *Inorg. Chem.* **1977**, *16*, 1851.
(16) $(Et_4N)_2[Fe_4S_4(OPh)_4]$: Cleland, W. E.; Averill, B. A. *Inorg. Chim. Acta* **1981**, *56*, L9. Averill, B. A.; Ibers, J. A., unpublished results.
(17) Recent resonance Raman spectroscopic results for $(n\text{-}Bu_4N)_2[Fe_4S_4(SCH_2Ph)_4]$ suggest a different type of distortion of the cluster (Spiro, T. G., private communication). The crystal structure of this compound is not available.
(18) Berg, J. M.; Hodgson, K. O.; Holm, R. H. *J. Am. Chem. Soc.* **1979**, *101*, 4586.

0020-1669/83/1322-1550$01.50/0

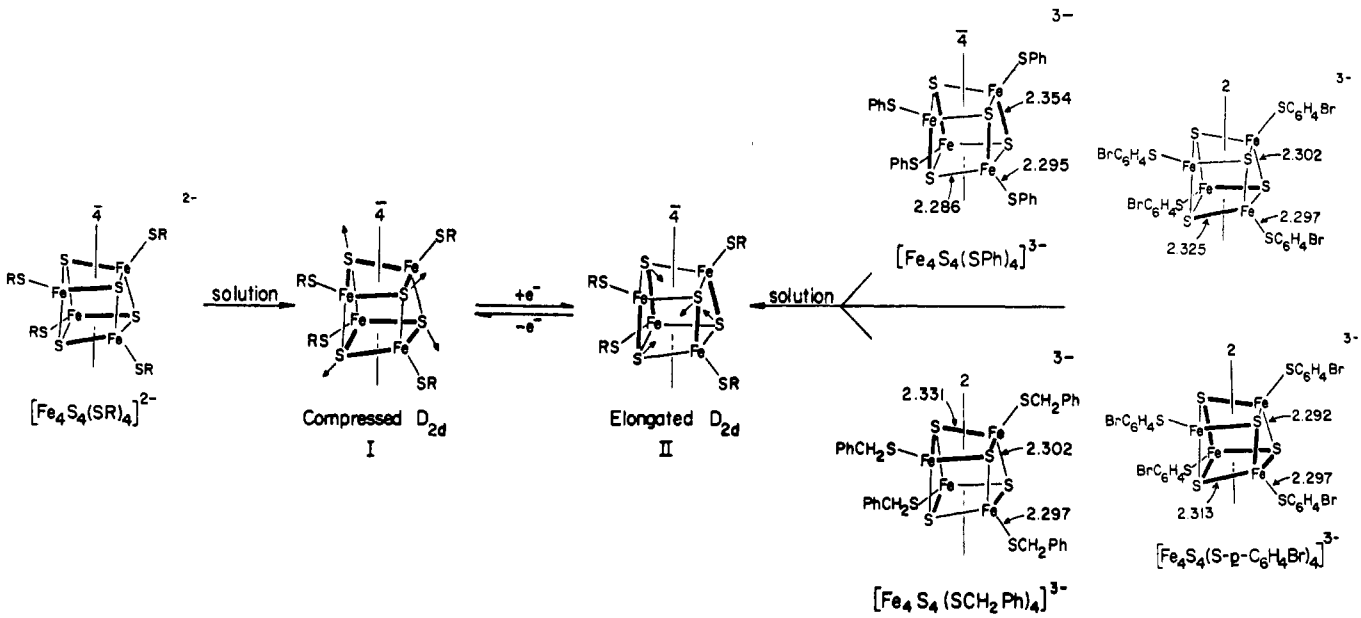

Figure 1. Schematic structures of $[Fe_4S_4(SR)_4]^{3-}$ clusters in the crystalline state and a simplified representation of the structural conversion of the Fe_4S_4 core in $[Fe_4S_4(SR)_4]^{2-,3-}$ electron transfer in solution. Idealized or actual core symmetry axes and mean values of Fe–SR and sets of longer (dark lines) and shorter Fe–S bonds are shown.

cluster has an elongated D_{2d} configuration. If it is accepted that a frozen solution is less likely to provide perturbing influences than is a crystalline phase, the elongated D_{2d} structure appears to be the intrinsically stable form of the [4Fe–4S]$^+$ core.

The properties of the analogue couple (2) are relevant to the biological couple (1) in that they are not influenced by protein structure and environment. As in other aspects of the synthetic analogue approach to metalloprotein site structures,[3,19] analogue properties are intrinsic and provide a base line against which protein influences can be assessed. With the clusters $[Fe_4S_4(SR)_4]^{3-}$ in the solid state, however, the foregoing evidence shows that their properties are influenced by the environment, perhaps accidentally simulating to an extent protein effects on [4Fe–4S]$^+$ cores. This raises the questions of the variability of core distortions, sensitivity of electronic properties to structure, and the generality of formation of the elongated D_{2d} solution structure from nontetragonal solid-state structures. Examination of these matters has been impeded by the considerable difficulty in obtaining single crystals of reduced cluster salts suitable for accurate X-ray structural determinations. The compound $(Et_4N)_3[Fe_4S_4(S\text{-}p\text{-}C_6H_4Br)_4]$ has recently been obtained in a suitable crystalline form. Its structure is reported here together with certain spectroscopic information bearing on the preceding points.

Experimental Section

Preparation of Compounds. All manipulations were performed under a pure argon or dinitrogen atmosphere with use of degassed solvents.

$(Et_4N)_2[Fe_4S_4(S\text{-}p\text{-}C_6H_4Br)_4]$. This compound was prepared by direct tetramer synthesis using elemental sulfur as the source of sulfide.[20,21] Sodium (1.52 g, 66 mmol) was dissolved in 200 mL of methanol. To this solution was added 12.5 g (66 mmol) of *p*-bromobenzenethiol (Aldrich Chemical Co.) followed by 2.7 g (17 mmol) of ferric chloride dissolved in 30 mL of methanol and 0.53 g (17 mmol) of sulfur. The reaction mixture was stirred overnight and filtered into a solution of 2.1 g (10 mmol) of Et_4NBr in 50 mL of methanol. After collection by filtration the compound was crystallized once from acetonitrile/methanol, affording 2.1 g (41%) of pure product as black crystals. Anal. Calcd for $C_{40}H_{56}Br_4Fe_4N_2S_8$: C, 35.21; H, 4.14; Br, 23.43; Fe, 16.37; N, 2.05; S, 18.80. Found: C, 35.07; H, 4.10; Br, 23.26; Fe, 16.37; N, 2.01; S, 18.11. ^1H NMR (CD_3CN): δ 8.31 (*m*-H), 5.85 (*o*-H), 3.15 (NCH_2), 1.20 (NCH_2CH_3). Redox potentials (cyclic voltammetry, 200 mV/s, DMF solution, vs. SCE): $E(2-/3-) = -0.93$ V; $E(3-/4-) = -1.64$ V.

$(Et_4N)_3[Fe_4S_4(S\text{-}p\text{-}C_6H_4Br)_4]$. This compound was prepared by reduction of the preceding compound with sodium acenaphthylenide.[5] A 0.2 M solution of the reductant was prepared from 0.15 g of sodium and 1.00 g of sublimed acenaphthylene in 33 mL of hexamethylphosphoramide (HMPA). To a solution of 2.3 g (1.7 mmol) of $(Et_4N)_2[Fe_4S_4(S\text{-}p\text{-}C_6H_4Br)_4]$ and 0.35 g (1.7 mmol) of Et_4NBr in 30 mL of HMPA was added dropwise 10 mL of the sodium acenaphthylenide solution. After the reaction mixture was stirred overnight, 60 mL of THF was added. Cooling to −20 °C caused separation of black crystals. After the product (2.4 g, 96%) was collected by filtration, it was recrystallized on small scales from acetonitrile or acetonitrile/diethyl ether. Anal. Calcd for $C_{48}H_{76}Br_4Fe_4N_3S_8$: C, 38.57; H, 5.13; Br, 21.38; Fe, 14.95; N, 2.81; S, 17.16. Found: C, 38.32; H, 4.87; Br, 21.22; Fe, 15.06; N, 2.65; S, 17.24. ^1H NMR (CD_3CN): δ 10.50 (*m*-H), 3.15 (NCH_2), 1.29 (NCH_2CH_3). This compound is extremely sensitive to oxidation, especially in solution.

X-ray Data Collection and Reduction. Slow crystallization performed by diffusion of diethyl ether into a dilute acetonitrile solution yielded long black needles of $(Et_4N)_3[Fe_4S_4(S\text{-}p\text{-}C_6H_4Br)_4]$. Suitable single crystals, obtained by cutting the needles, were mounted in glass capillaries under an argon atmosphere. Diffraction experiments were performed on a Nicolet R3M diffractometer with graphite-monochromatized Mo Kα radiation. The initial orientation matrix was obtained from 14 machine-centered reflections selected from a rotation photograph. Determination of an orthorhombic crystal system was made from 21 carefully centered high-angle reflections ($20° < 2\theta < 25°$). Partial rotation photographs around each axis confirmed *mmm* or *mm*2 symmetry. The observed systematic absences from a second partial data set ($3° < 2\theta < 25°$) were consistent only with space group *Fdd*2, which was confirmed by solution and refinement of the structure. The 21 centered reflections were used to obtain the final lattice parameters and the orientation matrix. Machine parameters, crystal data, and data collection parameters are summarized in Table I. The crystal selected for data collection gave ω scans for several low-angle reflections with full widths at half-heights of <0.25°. Friedel pairs ($+h,+k,\pm l$) were collected for the first shell of data ($3° < 2\theta < 30°$); $+h,+k,+l$ data were collected over $30° < 2\theta < 45°$. Three standard reflections were recorded every 60 reflections. Their intensities showed a 5–14% decrease over the duration of data collection. A decay correction was applied to the data on the basis of these standards. The data were processed by using the SHELXTL and

(19) Ibers, J. A.; Holm, R. H. *Science* **1980**, *209*, 223.
(20) Christou, G.; Garner, C. D. *J. Chem. Soc., Dalton Trans.* **1979**, 1093.
(21) Hagen, K. S.; Reynolds, J. G.; Holm, R. H. *J. Am. Chem. Soc.* **1981**, *103*, 4054.

Table I. Summary of Crystal Data, Intensity Collection, and Structure Refinement of $(Et_4N)_3[Fe_4S_4(S\text{-}p\text{-}C_6H_4Br)_4]$

formula (mol wt)	$C_{48}H_{76}Br_4Fe_4N_3S_8$ (1494.66)
a, Å	36.218 (10)
b, Å	30.972 (7)
c, Å	11.631 (3)
cryst syst	orthorhombic
space group	$Fdd2$
Z	8
V, Å^3	13 046 (6)
d_{calcd}, g/cm^3	1.52
cryst dimens, mm	0.58 × 0.16 × 0.18
cryst faces	{110}, {011}
radiation	Mo Kᾱ (λ 0.710 69 Å)
abs coeff (μ), cm^{-1}	35.78
transmission factors	51.54 min, 60.63 max
scan speed, deg/min	2.0-29.3 ($\theta/2\theta$ scan)
scan range, deg	0.7 below $K\alpha_1$ to 1.0 above $K\alpha_2$
bkgd/scan time ratio	0.25
data collected	2θ of 3-30°, $+h,+k,\pm l$; 2θ of 30-45°, $+h,+k,+l$
unique data including Friedel pairs ($F_o^2 > 2\sigma(F_o^2)$)	1789
no. of variables	238
goodness of fit	1.456
R, %	6.39
R_w, %	6.11

SHELX-76 program packages (Nicolet XRD Corp., Fremont, CA). An analytical absorption correction was applied to the complete data set. A total of 1789 reflections with $F_o^2 > 2\sigma(F_o^2)$ including Friedel pairs was collected.

Structure Solution and Refinement. The positions of the two Fe atoms in the asymmetric unit were determined from a Patterson map. Bromine and sulfur (sulfido) atoms were located from subsequent difference Fourier maps. This partial solution was in agreement with that obtained by direct methods. The remaining non-hydrogen atoms of the cations and anion were found from addition difference Fourier maps. A block-diagonal refinement employing anisotropic descriptions of Fe, S, and Br atoms and isotropic C and N atoms gave $R = 8.9\%$. An analytical absorption correction was then applied. Several more cycles of refinement, in which the phenyl rings were constrained to be regular hexagons of isotropic description and the remaining atoms were treated anisotropically, gave $R = 7.5\%$. Repeated attempts to refine anisotropically the C atoms of the full cation (N(2)C(17-24)) in the asymmetric unit failed. The apparent high degree of thermal motion of the C atoms led to an isotropic description of these atoms in subsequent refinements. At this point the polarity of the data was inverted. A difference Fourier calculation showed $R = 6.59\%$, indicating that the second polarity is the correct choice. Subsequent refinements were performed by using this polarity of the data. Hydrogen atoms were calculated by assuming trigonal (phenyl rings) and tetrahedral (cations) geometries and a C–H distance of 0.96 Å. Temperature factors were set at 1.2 times the isotropic temperature factor of the bonded C atom. Following refinement cycles in which hydrogen contributions were included, H atom positions were recalculated. In the final block-cascade refinement including hydrogen atom contributions, the phenyl rings were constrained to rigid hexagons of anisotropic atoms. The mean shift of the parameters in the last cycle of refinement was 0.003σ. A final difference Fourier map showed no peaks of chemical significance. Final R factors are included in Table I.

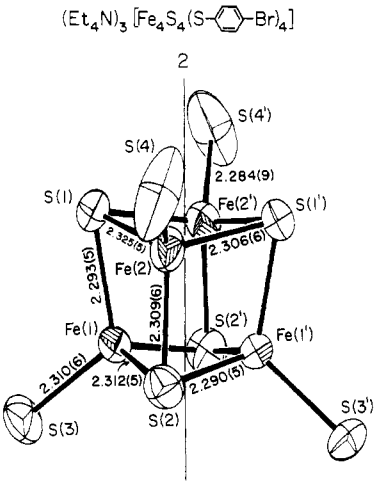

Figure 2. Structure of the Fe_4S_8 portion of $[Fe_4S_4(S\text{-}p\text{-}C_6H_4Br)_4]^{3-}$ as its Et_4N^+ salt, showing 50% probability ellipsoids, selected interatomic distances, and the atom-labeling scheme. Primed and unprimed atoms are related by the crystallographic twofold symmetry axis.

The following results for $(Et_4N)_3[Fe_4S_4(S\text{-}p\text{-}C_6H_4Br)_4]$ are tabulated: positional parameters (Table II), interatomic distances and angles of the anion (Table III), temperature factors (Table S-I), hydrogen atom coordinates and temperatures factors (Table S-II), best-weighted least-squares planes of the Fe_4S_4 core of the anion (Table S-III), values of $10|F_o|$ and $10|F_c|$ (Table S-IV[22]).

Table II. Positional Parameters (×10^4) for $(Et_4N)_3[Fe_4S_4(S\text{-}p\text{-}C_6H_4Br)_4]$

atom	x	y	z	atom	x	y	z
Fe(1)	133 (1)[a]	−415 (1)	0	C(8)	1216 (6)	939 (5)	−3911 (13)
Fe(2)	360 (1)	171 (1)	−1641 (3)	C(9)	1250 (6)	1343 (5)	−4434 (13)
S(1)	184 (1)	−542 (1)	−1936 (4)	C(10)	966 (6)	1645 (5)	−4338 (13)
S(2)	466 (1)	210 (2)	314 (4)	C(11)	648 (6)	1544 (5)	−3719 (13)
Br(1)[b]	1001 (1)	2165 (1)	−5101 (5)	C(12)	613 (6)	1141 (5)	−3196 (13)
Br(2)	−209 (1)	−2851 (1)	−85 (4)	C(13)	2475 (9)	2084 (8)	−2524 (25)
S(3)	372 (2)	−940 (2)	1200 (4)	C(14)	2455 (10)	1657 (7)	−3070 (22)
S(4)	870 (2)	308 (2)	−2736 (8)	C(15)[b]	2809 (11)	2452 (8)	−4044 (25)
N(1)	0	5000	9266 (23)	C(16)	3204 (11)	2458 (13)	−3374 (56)
N(2)	1213 (4)	1371 (6)	784 (20)	C(17)	1292 (6)	1824 (7)	1368 (22)
C(1)[b,c]	195 (4)	−1462 (4)	806 (16)	C(18)	986 (9)	2117 (10)	1388 (32)
C(2)	53 (4)	−1556 (4)	−281 (16)	C(19)	847 (8)	1217 (8)	1320 (21)
C(3)	−61 (4)	−1974 (4)	−544 (16)	C(20)	953 (15)	1117 (16)	2624 (47)
C(4)	−33 (4)	−2300 (4)	280 (16)	C(21)	1539 (7)	1129 (7)	1024 (23)
C(5)	108 (4)	−2207 (4)	1367 (16)	C(22)	1549 (9)	667 (11)	381 (32)
C(6)	222 (4)	−1788 (4)	1630 (16)	C(23)	1051 (12)	1432 (13)	−463 (36)
C(7)	897 (6)	838 (5)	−3292 (13)	C(24)	1401 (11)	1551 (14)	−1196 (43)

[a] Estimated standard deviations in parentheses in this and succeeding tables. [b] Numbering schemes of phenyl rings and cations:

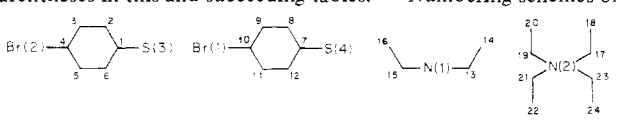

[c] The positions of C(1)-C(6) and C(7)-C(12) were calculated and refined on the basis of rigid-body phenyl rings. A regular hexagon with C-C distances of 1.395 Å was employed.

Table III. Selected Interatomic Distances (Å) and Angles (deg) in $[Fe_4S^*_4(S\text{-}p\text{-}C_6H_4Br)_4]^{3-}$

		Fe-S	
Fe(1)-S(3)	2.310 (6)	Fe(2)-S(4)	2.284 (9)
		Fe-S*	
Fe(1)-S(1)	2.293 (5)	Fe(2)-S(2)	2.309 (6)
Fe(1)-S(2)	2.312 (5)	Fe(2)-S(1′)	2.306 (6)
Fe(1)-S(2′)	2.290 (5)	mean	2.306 (13)[a]
Fe(2)-S(1)	2.325 (5)		
		Fe···S*	
Fe(1)-S(1′)	3.897 (5)	Fe(2)-S(2)	3.938 (6)
		Fe···Fe	
Fe(1)-Fe(2)	2.760 (3)	Fe(2)-Fe(2′)	2.814 (6)
Fe(1)-Fe(1′)	2.748 (5)	mean[b]	2.754 (35)
Fe(1)-Fe(2′)	2.720 (3)		
		S*···S*	
S(1)-S(2)	3.650 (7)	S(2)-S(2′)	3.618 (10)
S(1)-S(1′)	3.613 (9)	mean[b]	3.644 (24)
S(1)-S(2′)	3.667 (7)		
		Fe-S*-Fe	
Fe(1)-S(1)-Fe(2)	73.4 (2)	Fe(2)-S(2)-Fe(1′)	72.5 (2)
Fe(1)-S(1)-Fe(2′)	72.5 (2)	Fe(1)-S(2)-Fe(1′)	73.3 (2)
Fe(2)-S(1)-Fe(2′)	74.8 (2)	mean	73.3
Fe(1)-S(2)-Fe(2)	73.4 (2)		
		S*-S*-S*	
S(2)-S(1)-S(1′)	60.6 (1)	S(1)-S(2)-S(2′)	60.6 (1)
S(2)-S(1)-S(2′)	59.3 (2)	S(1′)-S(2)-S(2′)	60.1 (1)
S(1′)-S(1)-S(2′)	60.2 (1)	mean	60.0
S(1)-S(2)-S(1′)	59.2 (2)		
		S*-Fe-S*	
S(1)-Fe(1)-S(2)	104.9 (2)	S(2)-Fe(2)-S(1′)	105.2 (2)
S(1)-Fe(1)-S(2′)	106.3 (2)	S(1)-Fe(2)-S(1′)	102.6 (2)
S(2)-Fe(1)-S(2′)	103.7 (2)	mean	104.4
S(1)-Fe(2)-S(2)	103.9 (2)		
		Fe-Fe-Fe	
Fe(2)-Fe(1)-Fe(1′)	59.2 (1)	Fe(1)-Fe(2)-Fe(2′)	58.4 (1)
Fe(2)-Fe(1)-Fe(2′)	61.8 (1)	Fe(1′)-Fe(2)-Fe(2′)	59.8 (1)
Fe(1′)-Fe(1)-Fe(2′)	60.6 (1)	mean	60.0
Fe(1)-Fe(2)-Fe(1′)	60.2 (1)		
		S-Fe-S*	
S(3)-Fe(1)-S(1)	116.3 (2)	S(4)-Fe(2)-S(2)	113.9 (3)
S(3)-Fe(1)-S(2)	107.4 (2)	S(4)-Fe(2)-S(1′)	121.0 (3)
S(3)-Fe(1)-S(2′)	116.9 (2)	mean	114.0
S(4)-Fe(2)-S(1)	108.4 (3)		
		S-C	
S(3)-C(1)	1.80 (1)	S(4)-C(7)	1.76 (2)
		C-Br	
C(10)-Br(1)	1.84 (2)	C(4)-Br(2)	1.87 (1)

[a] The standard deviation of the mean was estimated from $\sigma \approx s = [(\Sigma x_i^2 - n\bar{x}^2)/(n-1)]^{1/2}$; no value is given for any angular quantity, as the variations exceed those expected for a sample taken from the same population. [b] Value for six distances.

Other Physical Measurements. Mössbauer spectral measurements were made with a conventional constant acceleration spectrometer having a ^{57}Co source in a rhodium matrix maintained at the same temperature as the absorber. Helium exchange gas provided thermal contact with the cryogenic liquid baths down to 4.2 K. Axial magnetic fields were applied with the use of a Nb_3Sn superconducting magnet operating in persistent mode up to 80 kOe and equipped with an oppositely wound backup coil to ensure a vanishing magnetic field at the site of the source. Isomer shifts are referenced to iron metal at 4.2 K. Electrochemical and X-band EPR determinations were carried out with equipment described elsewhere.[5,23] All measurements were performed under rigorously anaerobic conditions.

Results and Discussion

Description of the Structure. $(Et_4N)_3[Fe_4S_4(S\text{-}p\text{-}C_6H_4Br)_4]$ crystallizes with well-separated cations and anions in orthorhombic space group *Fdd*2. Dimensions of cations and *p*-C_6H_4Br groups are unexceptional and are not further considered. The structure of the Fe_4S_8 portion of the anion is presented in Figure 2. Selected interatomic distances and angles are compiled in Table III. A comparison of certain structural parameters with those of other $[Fe_4S_4(SR)_4]^{2-,3-}$ clusters is presented in Table IV, which contains data for the two 3- cluster structures previously available. The following are the principal structural features of $[Fe_4S_4(S\text{-}p\text{-}C_6H_4Br)_4]^{3-}$: (i) A crystallographically imposed twofold axis passes through core faces Fe(1,1′)S(2,2′) and Fe(2,2′)S(1,1′); this is the only instance of a symmetry element imposed on a $[Fe_4S_4(SR)_4]^{2-,3-}$ cluster. (ii) Fe_2S_2 core faces are decidedly nonplanar rhombs; the four independent core diagonal planes are nearly perfect (±0.01–±0.03 Å deviations from best-weighted least-squares planes[22]). (iii) Relative to $[Fe_4S_4(SPh)_4]^{2-}$ (or any other 2- cluster), mean values of all distances increase. In particular, the mean terminal Fe–S distance is ~0.04 Å longer. (iv) The volume of the Fe_4S_4 core is 2.2% larger than that in $[Fe_4S_4(SPh)_4]^{2-}$, an increase mainly due to a 2.9% larger S_4 volume. Features iii and iv are also found in $[Fe_4S_4(SCH_2Ph)_4]^{2-,3-}$ structural comparisons.[4,18] (v) Under the C_2 symmetry of (i), core Fe···Fe, S···S, and Fe–S distances divide into 4, 4, and 6 independent values, respectively. Of the last, the longest is Fe(2)–S(1), 2.325 (5) Å, and the shortest is Fe(1′)–S(2), 2.290 (5) Å. Other distances occur in the range 2.293 (5)–2.312 (5) Å. In the structures of $[Fe_4S_4(SCH_2Ph)_4]^{3-}$ [18] and, particularly, $[Fe_4S_4(SPh)_4]^{3-}$,[7] core Fe–S distances sort into "long" and "short" categories, leading to the simplified descriptions of core distortions in Figure 1. A unique description of this kind is not as clearcut for $[Fe_4S_4(S\text{-}p\text{-}C_6H_4Br)_4]^{3-}$ because bond distances are not as cleanly partitioned.[25] However, if such a description is pursued, there are two reasonable divisions: the two 2.325-Å bonds are taken as uniquely long, and the 10 other bonds are regarded as short with a mean value of 2.302 (9) Å; the four bonds of distances 2.290 and 2.293 Å with a mean value of 2.292 (2) Å are taken as short, and the eight remaining bonds (2.306 (6)–2.325 (5) Å) are considered long with a mean value of 2.313 (8) Å. Both of these descriptions are entered in Figure 1. (vi) With use of the mathematical model developed and applied previously,[7,10,18] the cores of $[Fe_4S_4(S\text{-}p\text{-}C_6H_4Br)_4]^{3-}$ and $[Fe_4S_4(SPh)_4]^{3-}$ are found to be maximally congruent when the twofold axis of the former and the $\bar{4}$ axis of the latter are approximately parallel. This is the spatial disposition shown in Figure 1. For $[Fe_4S_4(S\text{-}p\text{-}C_6H_4Br)_4]^{3-}$ and $[Fe_4S_4(SCH_2Ph)_4]^{3-}$ the maximally congruent orientation is that in which the twofold axes are approximately perpendicular. In neither pair of orientations is the maximum of long bonds aligned, a matter which emphasizes the small but different distortions of the three reduced clusters from idealized T_d core symmetry.

Mössbauer Spectra. The Et_4N^+ salts of $[Fe_4S_4(S\text{-}p\text{-}C_6H_4Br)_4]^{2-,3-}$ have been examined in the solid (2-) and in the solid and solution states (2-, 3-). Spectral parameters, collected in Table V, were obtained by least-squares fits of the experimental data to calculated spectra assuming Lorentzian line shapes. All zero-field spectra were fit with a two-site model.

(22) See paragraph at the end of this article regarding supplementary material.
(23) Mascharak, P. K.; Papaefthymiou, G. C.; Frankel, R. B.; Holm, R. H. *J. Am. Chem. Soc.* **1981**, *103*, 6110.
(24) Tetrahedral radii: Fe(II), 0.77 Å; Fe(III), 0.63 Å (Shannon, R. D. *Acta Crystallogr., Sect. A* **1976**, *A32*, 751).
(25) Compare the Fe–S bond length data in Tables III and IV with the following ranges for other clusters. $[Fe_4S_4(SPh)_4]^{3-}$: long, 2.337 (6)–2.368 (6) Å (anion 1), 2.342 (6)-2.354 (6) Å (anion 2); short, 2.272 (6)–2.299 (6) Å (anion 1), 2.280 (6)–2.300 (6) Å (anion 2).[7] $[Fe_4S_4(SCH_2Ph)_4]^{3-}$: long, 2.325 (5)–2.334 (5) Å; short, 2.296 (5)–2.308 (5) Å.[18]

Table IV. Selected Structural Features of $[Fe_4S^*_4(SR)_4]^{2-,3-}$ Clusters

cluster	dist, Å				vol, Å^3			
	Fe···Fe	Fe-S*	S···S	Fe-S	Fe_4	S_4	Fe_4S_4	ref
$[Fe_4S_4(S\text{-}p\text{-}C_6H_4Br)_4]^{3-}$	2.754[c]	2.313 (8)[a,e]	3.659 (2)	2.297	2.46	5.70	9.76	*b*
		2.292 (4)	3.616 (4)					
$[Fe_4S_4(SPh)_4]^{3-}$[d]	2.750 (4)	2.351 (4)	3.685 (4)	2.295	2.43	5.76	9.73	4, 7
	2.730 (2)	2.288 (8)	3.605 (2)					
$[Fe_4S_4(SCH_2Ph)_4]^{3-}$	2.759[c]	2.316 (6)	3.702 (2)	2.297	2.48	5.80	9.86	4, 18
		2.302 (6)	3.647 (4)					
$[Fe_4S_4(SPh)_4]^{2-}$	2.736 (4)	2.296 (8)	3.850 (2)	2.263	2.41	5.54	9.55	4, 11
	2.730 (2)	2.267 (4)	3.592 (4)					

[a] The number of values averaged is given in parentheses where two distances are shown; otherwise, the mean of all distances is given. [b] This work. [c] Because of the irregular structure, the mean of all values is given. [d] Average values of two independent anions given. [e] An alternative division of long and short distances is 2.325[2] and 2.302 Å.[10]

Table V. Mössbauer Spectral Parameters of $[Fe_4S_4(SR)_4]^{2-,3-}$ Clusters

compd	*T*, K	parameters, mm/s			rel intens[b,c]
		δ[a]	ΔE_Q	Γ[b]	
$(Et_4N)_2[Fe_4S_4(S\text{-}p\text{-}C_6H_4Br)_4]$	4.2	0.34 ± 0.02	1.77 ± 0.04	0.28	0.39
solid		0.33 ± 0.02	0.95 ± 0.04	0.28	0.61
	77	0.33 ± 0.02	1.08 ± 0.04	0.28	0.43
		0.32 ± 0.02	0.77 ± 0.04	0.28	0.57
$(Et_4N)_3[Fe_4S_4(S\text{-}p\text{-}C_6H_4Br)_4]$	4.2	0.48 ± 0.03	2.07 ± 0.06	0.56	0.57
solid		0.43 ± 0.03	0.94 ± 0.06	0.62	0.43
CH_3CN soln[d]	4.2	0.51 ± 0.03	1.91 ± 0.06	0.62	0.40
		0.45 ± 0.03	1.12 ± 0.06	0.64	0.60
DMF soln[d]	4.2	0.50 ± 0.05	1.84 ± 0.09	0.70	0.42
		0.47 ± 0.05	1.09 ± 0.09	0.70	0.58
	77	0.49 ± 0.05	1.58 ± 0.08	0.44	0.29[f]
		0.44 ± 0.05	0.99 ± 0.08	0.44	0.71
$(Et_3MeN)_3[Fe_4S_4(SPh)_4]$	4.2	0.50 ± 0.02	1.98 ± 0.03	0.55	0.45
solid[e]		0.46 ± 0.02	1.10 ± 0.03	0.67	0.55
$(Et_4N)_3[Fe_4S_4(SPh)_4]$	4.2	0.51 ± 0.02	2.01 ± 0.03	0.64	0.44
CH_3CN soln[d,e]		0.45 ± 0.02	1.11 ± 0.03	0.55	0.56
DMF soln[d]	4.2	0.50 ± 0.03	1.85 ± 0.06	0.76	0.55
		0.46 ± 0.03	1.06 ± 0.06	0.64	0.45
	77	0.47 ± 0.03	1.48 ± 0.05	0.46	0.36[f]
		0.43 ± 0.03	0.95 ± 0.05	0.40	0.64

[a] Relative to Fe metal at 4.2 K. [b] All fits were obtained with unconstrained parameters except for the condition of equal line widths for components of the same doublet. [c] ±0.05 to ±0.07. [d] 15-30 mM. [e] Reference 7. [f] Satisfactory fits were also obtained by constraining the intensity ratio to be ~1:1.

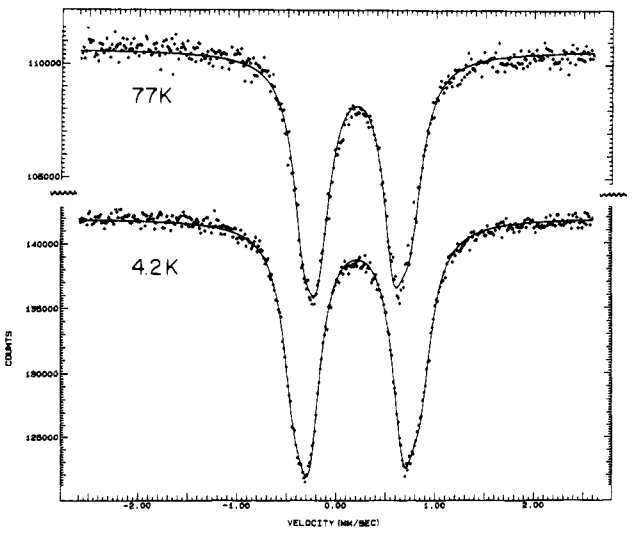

Figure 3. Mössbauer spectra of $(Et_4N)_2[Fe_4S_4(S\text{-}p\text{-}C_6H_4Br)_4]$ at 77 and 4.2 K. The solid lines are the least-squares fits of calculated spectra to the experimental data for two (slightly inequivalent) quadrupole doublets.

(a) $(Et_4N)_2[Fe_4S_4(S\text{-}p\text{-}C_6H_4Br)_4]$. Spectra of polycrystalline samples in zero field at 4.2 and 77 K are given in Figure 3. At the lower temperature two overlapping quadrupole doublets are evident; the site inequivalence persists at 77 K. Within experimental uncertainty both sites have the same isomer shift

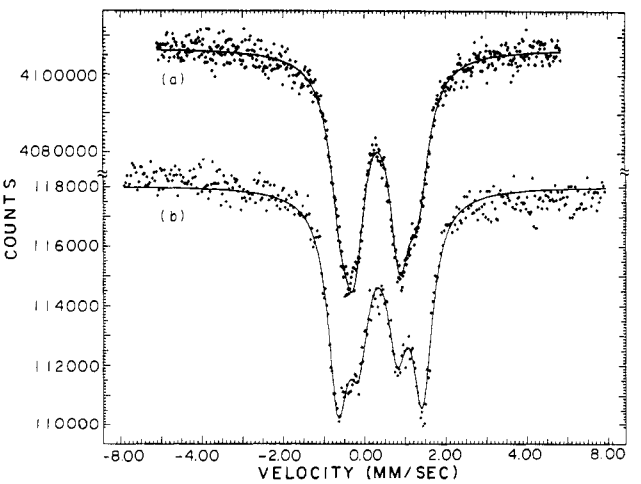

Figure 4. Mössbauer spectra of $(Et_4N)_3[Fe_4S_4(S\text{-}p\text{-}C_6H_4Br)_4]$ at 4.2 K: (a) ~15 mM solution in acetonitrile; (b) polycrystalline powder. The solid lines have the meaning of those in Figure 3.

(δ) but different quadrupole splittings (ΔE_Q). Identical isomer shifts (0.33 ± 0.02 mm/s) indicate that the two sites are not associated with inequivalent Fe oxidation states. As with other $[Fe_4S_4(SR)_4]^{2-}$ clusters,[26,27] the [4Fe-4S]$^{2+}$ core is electron-

(26) Frankel, R. B.; Averill, B. A.; Holm, R. H. *J. Phys. (Orsay, Fr.)* **1974**, *35*, C6-107.

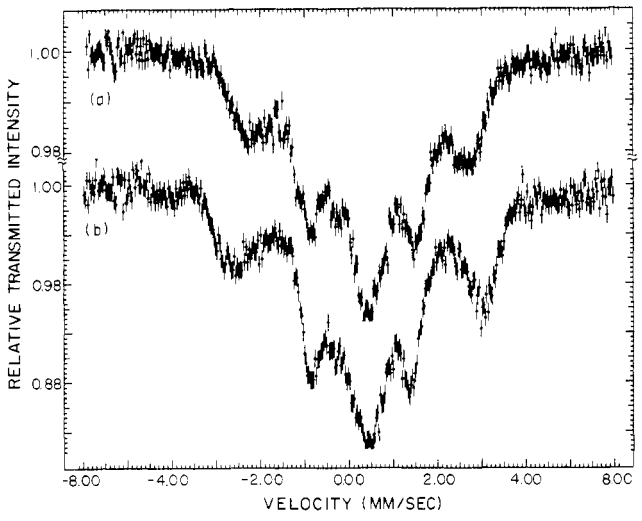

Figure 5. Mössbauer spectra of polycrystalline $(Et_4N)_3[Fe_4S_4(S\text{-}p\text{-}C_6H_4Br)_4]$ at 4.2 K in external magnetic fields applied parallel to the γ-ray direction: (a) H_0 = 60 kOe; (b) H_0 = 80 kOe.

ically delocalized with all four Fe atoms described by the mean oxidation state $Fe^{2.5+}$. This situation approaches the limiting case of $(Et_4N)_2[Fe_4S_4(SCH_2Ph)_4]$.[26,27] Strict equivalence of all Fe sites was observed from 1.5 K to room temperature (δ = 0.34 mm/s; ΔE_Q = 1.25 mm/s at 1.5–77 K), with a relatively narrow line width Γ = 0.25 mm/s at 77 K.

(b) $(Et_4N)_3[Fe_4S_4(S\text{-}p\text{-}C_6H_4Br)_4]$. Zero-field spectra of the reduced cluster at 4.2 K in the solid state and in acetonitrile solution are presented in Figure 4. The solid-state spectrum arises from superposition of two doublets of roughly equal intensities, similar isomer shifts, and quite different quadrupole splittings. The appearance of two doublets in the solid-state spectrum is consistent with cluster C_2 crystallographic symmetry, which affords two types of Fe sites, Fe(1,1′) and Fe(2,2′). Isomer shifts of the two sites (δ_1 = 0.43 mm/s, δ_2 = 0.48 mm/s) fall within the range 0.43–0.52 mm/s observed for other $[Fe_4S_4(SR)_4]^{3-}$ clusters.[7,8] This cluster is also electronically delocalized, with the δ values corresponding to the mean oxidation state $Fe^{2.25+}$. The line widths of the doublets are comparable with those of other reduced clusters at 4.2 K.[7,8] However, the difference in quadrupole splittings, 1.13 mm/s, is 0.2–1.1 mm/s larger than for those clusters. This, rather than intrinsically narrower absorption lines,[28] accounts for the spectrum being by far better resolved than that of any other reduced cluster yet observed.[7,8]

Because of improved spectral resolution the electronic nature of $[Fe_4S_4(S\text{-}p\text{-}C_6H_4Br)_4]^{3-}$ has been examined, by use of magnetically perturbed spectra, in somewhat more detail than for other reduced clusters.[7,8] The application of an external magnetic field induces magnetic hyperfine structure, resulting in the spectra in Figure 5. The complexity and broadening of these spectra arise primarily from unequal hyperfine coupling constants at the Fe sites, different orientations of the principal components of the electric field gradients (EFG) in the powder sample relative to the applied field, and a distribution of internal hyperfine fields owing to the orientation dependence of the hyperfine interaction. The two pairs of outer lines that flank the central unresolved absorption feature move in opposite directions as the applied field is increased from 60 to 80 kOe. This behavior is consistent with antiferromagnetic

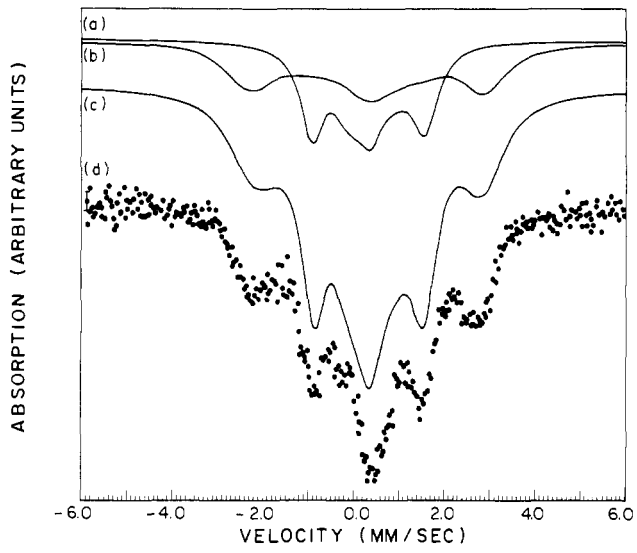

Figure 6. Mössbauer spectra of polycrystalline $(Et_4N)_3[Fe_4S_4(S\text{-}p\text{-}C_6H_4Br)_4]$ at 4.2 K in an external magnetic field of 60 kOe applied parallel to the γ-ray direction: (a) simulated spectrum of site 1 with δ_1 = 0.43 mm/s, ΔE_{Q_1} = 0.94 mm/s, Γ_1 = 0.62 mm/s, $H_{eff(1)}$ = −52 kOe; (b) simulated spectrum of site 2 with δ_2 = 0.48 mm/s, ΔE_{Q_2} = −2.07 mm/s, Γ_2 = 1.12 mm/s, $H_{eff(2)}$ = 102 kOe; (c) superposition of spectra a and b in a 1:1 intensity ratio; (d) experimental spectrum. For clarity spectra a and b are not drawn to the scale of spectrum c.

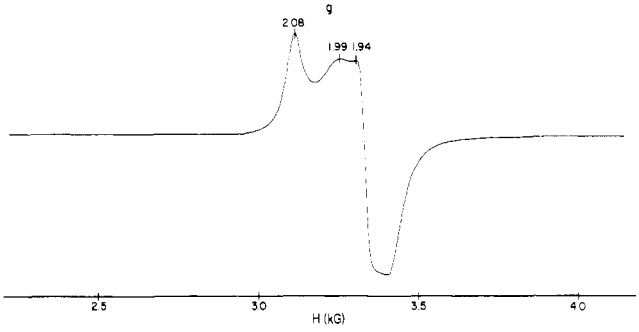

Figure 7. Solid-state X-band EPR spectrum of $(Et_4N)_3[Fe_4S_4(S\text{-}p\text{-}C_6H_4Br)_4]$ at ~7 K.

spin coupling, which is a general property of reduced clusters and has been theoretically analyzed recently.[29] The overall magnitude of the splittings at the two magnetic subsites is roughly comparable to those in the less well-resolved spectra of several $[Fe_4S_4(SR)_4]^{3-}$ species (R = Ph, *o*-tolyl) in the solid state.[7] The splittings are also similar to those observed in reduced *Bacillus stearothermophilus* ferredoxin.[30]

To obtain estimates of the effective fields (H_{eff}) at the Fe sites, the magnetically perturbed spectra were simulated by superposition of two sites of equal intensity corresponding to those observed at 4.2 K in the absence of an applied field. In Figure 6 the experimental spectrum at 60 kOe is presented together with simulated spectra. The latter were obtained by averaging over a random orientation of the molecular axes at the Fe sites relative to the applied field direction, as required for a powder sample. The number of parameters was minimized by considering only the case of an axially symmetric EFG (asymmetry parameter η = 0). Parameters used in the simulation of the spectra of sites 1 and 2 are specified in Figure

(27) Holm, R. H.; Averill, B. A.; Herskovitz, T.; Frankel, R. B.; Gray, H. B.; Siiman, O.; Grunthaner, F. J. *J. Am. Chem. Soc.* **1974**, *96*, 2644.
(28) Site 1, with the marginally larger line width, is associated with the site of the larger hyperfine field observed in the spectrum of this compound in an applied magnetic field. This observation (vide infra) suggests that the lines are broadened by incipient magnetic hyperfine interactions.
(29) Papaefthymiou, G. C.; Laskowski, E. J.; Frota-Pessôa, S.; Holm, R. H. *Inorg. Chem.* **1982**, *21*, 1723.
(30) Middleton, P.; Dickson, D. P. E.; Johnson, C. E.; Rush, J. D. *Eur. J. Biochem.* **1978**, *88*, 135.

6. The δ and ΔE_Q values are taken from the zero-field spectra at 4.2 K. The line widths of site 2, however, are considerably broadened (from 0.56 to 1.12 mm/s). This is due to the fact that site 2 has the larger quadrupole splitting, and line broadening is expected to be introduced by the spatial averaging of a random distribution of the EFG axes relative to the applied field direction. However, the large extent of broadening observed indicates that in addition there exists a distribution of effective hyperfine fields at that site. For simplicity this distribution was approximated by a single average value of H_{eff} and a broadened line width. From the differential broadening of the outermost absorption lines of the individual subcomponents, the sign of the principal component of each EFG was determined. At site 2 H_{eff} is positive (parallel to the applied field direction), and at site 1 it is negative. On the assumption that the electronic spins of the magnetic sites are aligned with or opposite to the direction of the applied field, the hyperfine fields are estimated as $H_{hf(1)} \cong -112$ kOe and $H_{hf(2)} \cong 42$ kOe. A similar analysis of the 80-kOe spectrum gave $H_{hf(1)} \cong -125$ kOe and $H_{hf(2)} \cong 45$ kOe. The existence of sites with different hyperfine fields, together with associated Mössbauer spectral properties and antiferromagnetic interactions among these sites,[29] is consistent with the spin-coupled model of the electronic structure of the $[4Fe-4S]^+$ oxidation level.[30]

Comparative Solid-State/Solution Properties. We have previously classified $[Fe_4S_4(SR)_4]^{3-}$ clusters in the solid state as having tetragonal or nontetragonal core structures on the basis of their electronic properties,[8] including those from Mössbauer and EPR spectra. This classification is not intended as literal, for a continuum of core structures ranging from varying degrees of rhombicity to the tetragonal limit is possible. Nonetheless, the collective properties in conjunction with established tetragonal and nontetragonal structures (Figure 1) have led to a self-consistent partitioning of the clusters into the two categories. An important qualification, evident in our earlier presentations,[7,8] is reemphasized. Crystal structure determinations of all reduced cluster compounds have been performed at ambient temperature. Magnetic and spectroscopic features correlated with tetragonal or nontetragonal $[4Fe-4S]^+$ core structures have been measured at ≤ 77 K and frequently at 4.2 K. Clearly, retention of the essential core structure at these lower temperatures is required for a valid property/structure correlation.

Mössbauer spectral criteria at 4.2 K for the two core structural categories are the following:[8] tetragonal—two overlapping quadrupole doublets with δ, ΔE_Q = 0.50–0.52, ~1.9–2.0 and 0.43–0.45, ~1.1 mm/s; nontetragonal—δ, ΔE_Q = 0.43–0.48, ~0.9–1.4 mm/s. The spectral parameters of $[Fe_4S_4(S\text{-}p\text{-}C_6H_4Br)_4]^{3-}$ in the solid state more closely approach those of the tetragonal category, a matter illustrated by comparison with the data for $(Et_3MeN)_3[Fe_4S_4(SPh)_4]$ in Table V. EPR spectra at X-band have also been found to correlate with structures:[8] tetragonal—nearly isotropic or axial, absorption at 3.0–3.8 kG; nontetragonal—complex, absorption extending over ca. 0.5–7 kG. Recent EPR lineshape simulations,[31] together with magnetic susceptibility results,[7,8] indicate that spectra of the latter type can arise wholly or partially from clusters with $S > {}^1/_2$. The spectrum of $(Et_4N)_3[Fe_4S_4(S\text{-}p\text{-}C_6H_4Br)_4]$ shown in Figure 7 falls nearer to those in the tetragonal category. Given the nontetragonal structure of this cluster, these observations extend the range of Mössbauer and EPR properties associated with this structural category. However, the Mössbauer and EPR spectra of this compound and those of $(Et_3MeN)_3[Fe_4S_4(SPh)_4]$,[7] containing the only structurally characterized tetragonal cluster, are distinguishable.

The Mössbauer spectra of $[Fe_4S_4(S\text{-}p\text{-}C_6H_4Br)_4]^{3-}$ in acetonitrile, DMF, and *N,N'*-dimethylacetamide solutions at 4.2–77 K are essentially identical. The spectra in Figure 4 reveal a striking difference between the solid and solution states. In the latter, two quadrupole doublets are evident but are unresolved, a situation due in part to the smaller difference in ΔE_Q values of the two subsites in solution. The solution spectra are indistinguishable from those of all other $[Fe_4S_4(SR)_4]^{3-}$ clusters previously examined.[7,8] This situation can be appreciated by comparison of spectral parameters in Table V, which also demonstrates the near-identity of these spectra to that of solid $(Et_3MeN)_3[Fe_4S_4(SPh)_4]$. In acetonitrile solution at ~7 K the EPR spectrum reduces to a simple axial case, with $g_\parallel \cong 2.02$ and $g_\perp = 1.92$. This spectrum is the same as that observed for all other $[Fe_4S_4(SR)_4]^{3-}$ clusters in this solvent.

These results show that the structure of $[Fe_4S_4(S\text{-}p\text{-}C_6H_4Br)_4]^{3-}$ in the solid and solution phases differs and that in solution the cluster approaches or adopts an elongated D_{2d} core configuration closely similar to that of $[Fe_4S_4(SPh)_4]^{3-}$ in a crystal of its Et_3MeN^+ salt.[7] Consequently, this work provides the second case of a structurally defined nontetragonal cluster undergoing a core structural change to a tetragonal form in solution. Including cases of known and unknown solid-state structures, $[Fe_4S_4(S\text{-}p\text{-}C_6H_4Br)_4]^{3-}$ is the sixth example overall. Thus, the generality of the unperturbed core structural alteration I $\rightleftharpoons$ II (Figure 1) attendant to the electron-transfer process (2) is further supported.

As observed earlier, the compressed tetragonal core structure I is a consistent feature of all structurally defined synthetic clusters with the $[4Fe-4S]^{2+}$ oxidation level.[10-16] The same type of distortion is apparent for four $[4Fe-4S]^{2+}$ protein clusters,[32-35] the most recent example being the site in *Azobacter vinelandii* ferredoxin I.[35] A comparison of the structures of analogue and protein clusters is available elsewhere.[4] Electronic structural calculations for a T_d core geometry of this oxidation level by Aizman and Case[36] yield a MO energy scheme in which the highest occupied orbital is filled. No static Jahn–Teller effect is expected, and the factors responsible for the D_{2d} geometry remain unclear. If the same scheme holds for the $[4Fe-4S]^+$ core in T_d symmetry, the odd electron would occupy a t_1 or t_2 orbital and Jahn–Teller distortion to a lower symmetry is possible. The three reduced clusters of known structure are distorted (Table IV). Their nonuniform core structures presumably originate in specific crystalline-state effects. In none of these cases have we been able to discern clearly, from crystal-packing diagrams or from interion distance calculations, interactions that might exert a perturbing influence on core structures. The existence of such interactions is well demonstrated by the essential degeneracy of the magnetic and spectroscopic properties of reduced clusters in frozen solutions. A detailed description of the structural interconversion I $\rightleftharpoons$ II, its effect on electron self-exchange rates of synthetic clusters, and the possible consequences for protein redox properties by constraints imposed on this interconversion are given elsewhere.[4,7-9,18]

Acknowledgment. This research was supported by National Institutes of Health Grant GM 28856 at Harvard University and by the National Science Foundation at the Francis Bitter

(31) Collison, D.; Mabbs, F. E. *J. Chem. Soc., Dalton Trans.* **1982**, 1565.
(32) Adman, E. T.; Sieker, L. C.; Jensen, L. H. *Acta Crystallogr., Sect. A* **1975**, *A31*, 534.
(33) Freer, S. T.; Alden, R. A.; Carter, C. W., Jr.; Kraut, J. *J. Biol. Chem.* **1975**, *250*, 46.
(34) Carter, C. W., Jr. *J. Biol. Chem.* **1977**, *252*, 7802.
(35) Ghosh, D.; O'Donnell, S.; Furey, W., Jr.; Robbins, A. H.; Stout, C. D. *J. Mol. Biol.* **1982**, *158*, 73.
(36) Aizman, A.; Case, D. A. *J. Am. Chem. Soc.* **1982**, *104*, 3269.

National Magnet Laboratory. We thank J. M. Berg for structural calculations and Dr. P. K. Mascharak for experimental assistance.

Registry No. **1**, 85269-29-0; $(Et_4N)_2[Fe_4S_4(S\text{-}p\text{-}C_6H_4Br)_4]$, 85269-27-8.

Supplementary Material Available: Tables S-I–S-IV, showing anisotropic temperature factors, hydrogen atom coordinates and isotropic temperature factors, best-weighted least-squares planes, and observed and calculated structure factors, and a stereoview of $(Et_4N)_3[Fe_4S_4(S\text{-}p\text{-}C_6H_4Br)_4]$ (15 pages). Ordering information is given on any current masthead page.

Notes

Contribution from the Department of Chemistry, Helsinki University of Technology, SF-02150 Espoo 15, Finland

Uranyl(VI) Compounds. 3.[1] Crystal Structures of Two Forms of Bis(urea)dioxouranium(VI) Sulfate[2]

Jukka Toivonen* and Lauri Niinistö

Received September 27, 1982

Uranyl sulfate forms several crystalline hydrates of the general formula $UO_2SO_4 \cdot nH_2O$. Detailed X-ray crystallographic studies of $UO_2SO_4 \cdot 2^1/_2H_2O$[3] and $UO_2SO_4 \cdot 3^1/_2H_2O$[4,5] have been carried out earlier. The structures consist of infinite double chains formed by alternating UO_7 and SO_4 polyhedra. In aqueous solution urea molecules are capable of replacing water molecules in the coordination sphere of the uranyl ion and complexes of the type $UO_2SO_4 \cdot nCO(NH_2)_2$ may be precipitated by evaporation. The replacement of water by urea leads to different networks as seen in the structures of the tris(urea)[6] and tetrakis(urea)[7] complexes. The former structure consists of single chains, whereas the latter is monomeric.

The X-ray crystallographic investigation carried out in this work has revealed that the bis(urea) complex forms two structurally related polymorphs. The crystal structures of the two polymorphs are described below.

Experimental Section

Crystals of both polymorphs of $UO_2SO_4 \cdot 2CO(NH_2)_2$ were obtained upon evaporation of an aqueous solution containing uranyl sulfate and urea in the molar ratio of 1:2 at room temperature. Chemical analysis showed that the crystals have the same composition. However, the polymorphs differed in color. The greenish and yellowish crystals were distinguished by the prefixes α and β, respectively. Fast evaporation yielded predominantly the β form. Preliminary DSC investigation revealed no polymorphic transitions for α and β forms.

The crystal data given in Table I are in agreement with the unit cell values for the β form given by Durski et al.[8] and with those reported recently by Serezhkin et al.;[9] the latter authors have also prepared the α form. The details of the intensity data collection with a Syntex $P2_1$ single-crystal diffractometer are included in Table I. Empirical absorption corrections were made from ψ-scan data, after which Lorentz and polarization corrections were applied to both sets of data.

Table I. Data for the X-ray Diffraction Study of $UO_2SO_4 \cdot 2CO(NH_2)_2$

	α-$UO_2SO_4 \cdot 2CO(NH_2)_2$	β-$UO_2SO_4 \cdot 2CO(NH_2)_2$
	(A) Crystal Data	
cryst syst	monoclinic	monoclinic
space group	$P2_1/c$	$P2_1/c$
a, Å	6.856 (1)	6.747 (1)
b, Å	12.760 (2)	14.110 (3)
c, Å	11.571 (1)	11.348 (1)
β, deg	91.73 (1)	106.53 (1)
V, Å^3	1011.80	1035.62
Z	4	4
cryst size, mm	0.15 × 0.15 × 0.3	0.15 × 0.15 × 0.25
fw	486.23	486.23
ρ(calcd), g cm^{-3}	3.191	3.118
ρ(obsd),[a] g cm^{-3}	3.14	3.08
μ(Mo Kα), cm^{-1}	157.9	154.3
cell const determn	25 reflctns, $35 < 2\theta < 40°$ [b]	25 reflctns, $35 < 2\theta < 40°$ [b]
	(B) Measurement of Intensity Data	
radiation	Mo Kα, graphite monochromator	
reflections measd	$+h, +k, \pm l$	
2θ range, deg	5–60	
scan type	$\theta/2\theta$	
scan speed, deg min^{-1}	2.0	
scan range, deg	$(2\theta(\text{Mo K}\alpha) - 1)$–$(2\theta(\text{Mo K}\alpha) + 1)$	
bkgd measmt	at beginning and end of the 2θ range, each for half of the total scan time	
no. of reflctns measd	3311	3376
std reflctns	$11\bar{1}$, 202	$\bar{1}41$, $\bar{2}02$
range of transmission factors	0.36–0.66	0.35–0.60
no. of unique data with $I > 3\sigma(I)$	2554	2587
extinction coeff g	0.00131 (4)	0.00129 (3)
$R = \Sigma \lvert\lvert F_o\rvert - \lvert F_c\rvert\rvert / \Sigma \lvert F_o\rvert$	0.060	0.069

[a] Measured by flotation. [b] λ(Mo Kα) = 0.7107.

The structures were solved by the heavy-atom method and refined by least-squares techniques using anisotropic temperature factors for all non-hydrogen atoms. In the final stages of the least-squares refinement the calculated positional parameters for all hydrogen atoms were introduced but not refined (fixed isotropic temperature factor U = 0.10 Å^2). The extinction correction was applied for both structures. Scattering factors for the non-hydrogen atoms were according to Cromer and Mann,[10] and those for hydrogen were according to Stewart et al.[11] Anomalous dispersion correction was applied for uranium.[12] Calculations were carried out with the X-RAY 76 program system.[13] The final positional parameters are given in Table II. Thermal parameters, hydrogen atom coordinates, and observed and calculated structure factors are available as supplementary material.

(1) For part 2 of the series see: Niinistö, L.; Toivonen, J.; Valkonen, J. *Acta Chem. Scand., Ser. A* **1979**, *A33*, 621.
(2) Presented in part at the 10th Scandinavian Meeting on Structural Chemistry, Helsinki, Jan 1981; see: "Book of Abstracts"; Association of Finnish Chemical Societies: Helsinki, Finland, 1981; p 76.
(3) Brandenburg, N. P.; Loopstra, B. O. *Cryst. Struct. Commun.* **1973**, *2*, 243.
(4) Putten, N.; Loopstra, B. *Cryst. Struct. Commun.* **1974**, *3*, 377.
(5) Zalkin, A.; Ruben, H.; Templeton, D. *Inorg. Chem.* **1978**, *17*, 3701.
(6) Ruben, H.; Spencer, B.; Templeton, D.; Zalkin, A. *Inorg. Chem.* **1980**, *19*, 776. See also: Serezhkin, V. N.; Soldatkina, M. A.; Trunov, V. K. *Radiokhimiya* **1981**, *23*, 678.
(7) Serezhkin, V. N.; Soldatkina, M. A.; Trunov, V. K. *Koord. Khim.* **1981**, *7*, 1880.
(8) Durski, Z.; Wojtaś, H.; Boniuk, H.; Nowaczek, H. *Acta Phys. Pol. A* **1978**, *A53*, 671.
(9) Soldatkina, M. A.; Serezhkin, V. N.; Serezhkina, L. B. *Zh. Neorg. Khim.* **1981**, *26*, 3029.
(10) Cromer, D.; Mann, J. *Acta Crystallogr., Sect. A* **1968**, *A24*, 321.
(11) Stewart, R. F.; Davidson, E. R.; Simpson, W. T. *J. Chem. Phys.* **1965**, *42*, 3175.
(12) Cromer, D. T.; Liberman, D. *J. Chem. Phys.* **1970**, *53*, 1981.
(13) Stewart, J. M., Ed. "*The X-Ray system, Version of 1976*" Technical Report TR-446; Computer Science Center, University of Maryland: College Park, MD, 1976.

0020-1669/83/1322-1557$01.50/0